As depicted in **Fig. S1**, the complete pressure-dependent enthalpy differences of Li_2YH_6 with respect to all considered decomposition pathways over the range of 50–300 GPa are presented. In contrast to the main text, where only a few representative pathways were retained to emphasize the primary physical trends, the full set of calculated pathways is displayed here in order to provide a more comprehensive view of the pressure responses of the different decomposition channels. It can be seen that the various pathways do not exhibit a uniform pressure dependence, but instead show clearly distinct evolutionary behaviors. Some channels display a pronounced decrease in enthalpy difference with increasing pressure, and even undergo sign changes in the intermediate-pressure region, indicating that their relative competitiveness is particularly sensitive to pressure. By contrast, other channels vary more gradually over the entire pressure range and show only limited enthalpy shifts, suggesting that their relative energetic ordering is comparatively stable. Overall, this complete pathway map indicates that the decomposition competition associated with Li_2YH_6 is not governed by a single pathway, but instead exhibits clear pathway dependence and pressure selectivity. For this reason, only several representative pathways that capture the main evolutionary trends were selected for presentation in the main text, while the complete results are provided in the Supplementary Information to preserve both the readability of the main text and the completeness of the thermodynamic analysis.

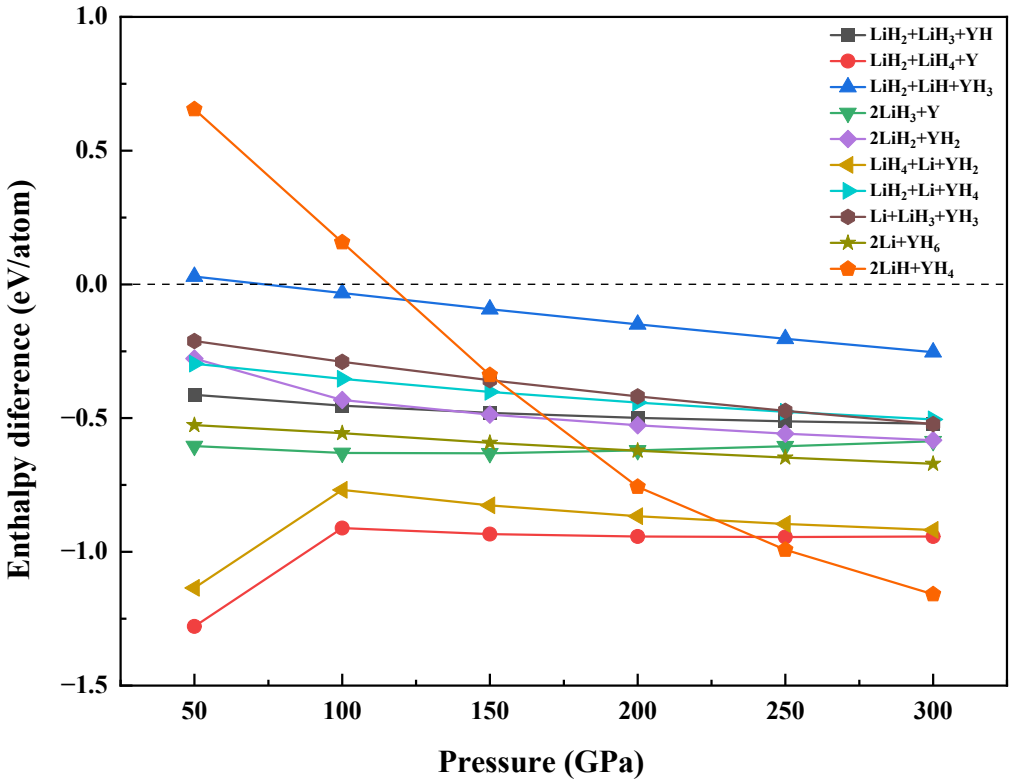

Figure S1. Complete pressure-dependent relative enthalpy differences of Li_2YH_6 with respect to all considered decomposition pathways over the pressure range of 50–300 GPa. Here, ΔH is defined as the enthalpy difference between Li_2YH_6 and the corresponding decomposition products for each pathway. Different pathways exhibit clearly distinct pressure responses, indicating pronounced pathway dependence in the thermodynamic competition. In contrast to the main text, where only several representative pathways are retained to highlight the main evolutionary trends, the full set of calculated pathways is presented here for completeness.

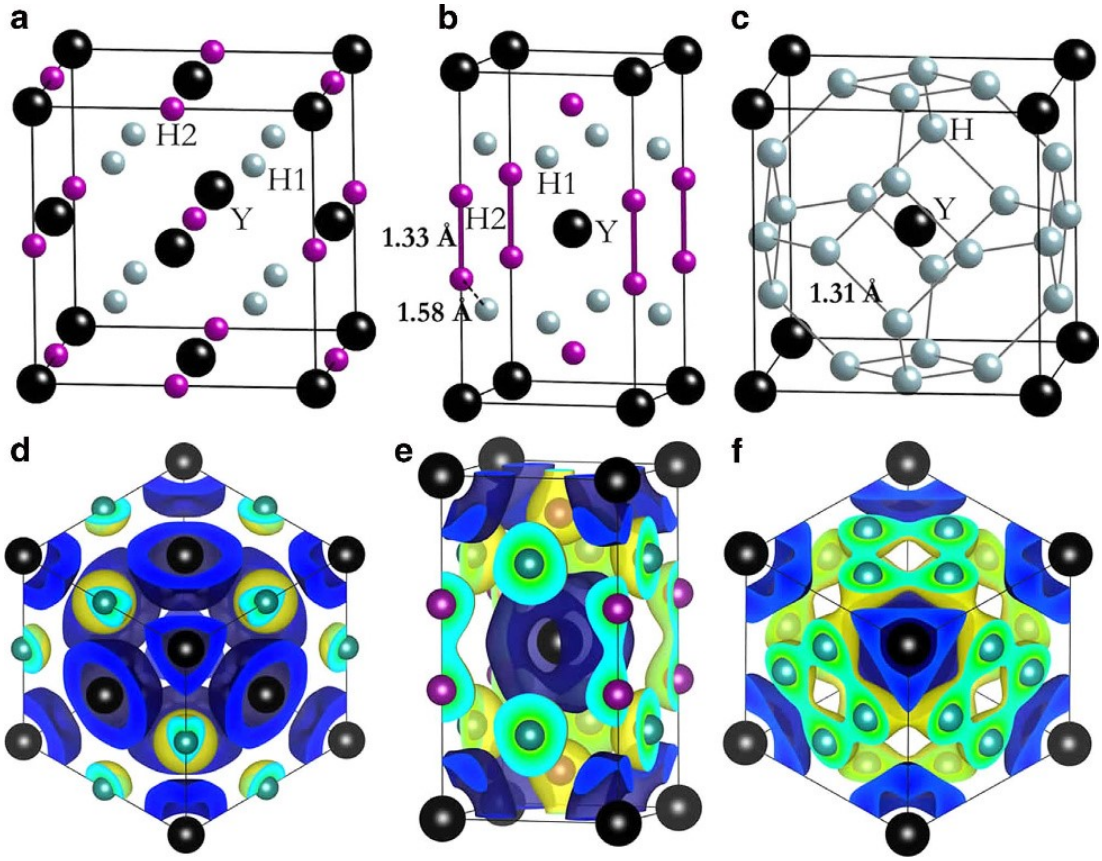

Figure S2. (b) Crystal structure of tetragonal *tI10*-YH_4 at 120 GPa (prototype used for comparison with Li_2YH_6). The lattice parameters are $a = 2.87$Å and $c = 5.33$Å. Y occupies the 2a (0, 0, 0) site, while the two nonequivalent H atoms H1 and H2 occupy 4d (0.5, 0, 0.75) and 4e (0, 0, 0.63), respectively. Reproduced from Ref. [38].

To further illustrate the structural evolution of Li_2YH_6 during variable-pressure relaxation, **Fig. S3** lists the optimized fractional atomic coordinates at 130, 170, and 180 GPa. It should be noted that the variable-pressure relaxations in this work were systematically performed in steps of 10 GPa; only three representative pressure points are shown here in order to reflect the overall trend across the studied pressure range. Among them, 130 GPa corresponds to the low-pressure end of the investigated interval, whereas 170 and 180 GPa are located in the high-pressure region and differ by 10 GPa, thus allowing a direct comparison of structural variations between adjacent pressure points. The results show that, throughout 130–180 GPa, the fractional atomic coordinates change only slightly, with the overall variations remaining essentially on the order of 10^{-3}–10^{-6}. This indicates that the I4/mmm structural framework remains stable during variable-pressure relaxation, without any obvious atomic rearrangement or symmetry breaking. This is consistent with the optimization results showing that Li_2YH_6 retains the I4/mmm symmetry throughout 130–180 GPa, and further supports the absence of any clear pressure-induced structural phase transition within this pressure range. Together with the phonon spectra showing no imaginary frequencies, these results support the good dynamical stability of this phase over the investigated pressure range.

(a)130GPa

```
ATOMIC_POSITIONS {crystal}
 H   0.9297000000000003    0.9297000000000001    0.0000000000000001
 H  -0.9297000000000003   -0.9297000000000002    0.0000000000000001
 H   0.1548400000000001    0.6548400000000003    0.5000000000000000
 H   0.6548400000000002    0.1548400000000000    0.5000000000000001
 H  -0.1548400000000001   -0.6548400000000001   -0.5000000000000001
 H   0.3451600000000000   -0.1548400000000002    0.5000000000000001
Li   0.2317700000000002    0.2317700000000001    0.0000000000000000
Li  -0.2317700000000000   -0.2317700000000000    0.0000000000000001
 Y   0.5000000000000001    0.5000000000000002    1.0000000000000004
```

(b)170GPa

```
ATOMIC_POSITIONS (crystal)
H         0.932436749   0.932436749  -0.000000000
H        -0.932436749  -0.932436749   0.000000000
H         0.156586337   0.656586337   0.500000000
H         0.656586337   0.156586337   0.500000000
H        -0.156586337  -0.656586337  -0.500000000
H         0.343413663  -0.156586337   0.500000000
Li        0.231537101   0.231537101  -0.000000000
Li       -0.231537101  -0.231537101   0.000000000
Y         0.500000000   0.500000000   1.000000000
```

(c)180GPa

```
ATOMIC_POSITIONS (crystal)
H         0.932436749   0.932436749   0.000000000
H        -0.932436749  -0.932436749   0.000000000
H         0.156586337   0.656586337   0.500000000
H         0.656586337   0.156586337   0.500000000
H        -0.156586337  -0.656586337  -0.500000000
H         0.343413663  -0.156586337   0.500000000
Li        0.231537102   0.231537102  -0.000000000
Li       -0.231537102  -0.231537102  -0.000000000
Y         0.500000000   0.500000000   1.000000000
```

Figure S3. Optimized fractional atomic coordinates of I4/mmm-Li_2YH_6 at representative pressures. Variable-pressure relaxations were performed in steps of 10 GPa; for brevity, only three representative pressure points, 130, 170, and 180 GPa, are shown here.

To further quantitatively analyze the connection between bonding heterogeneity and superconductivity-relevant physics, **Figs. S4** and **S5** present the Partial density of states and projected phonon density of states for distinct local hydrogen environments, respectively. **Fig. S4** shows that the H_2-like H retains a larger electronic-state contribution near E_F, indicating that the H_2-like unit is not merely a localized molecular-like motif far below the Fermi level, but also directly participates in the low-energy electronic structure. **Fig. S5** further shows that different local H environments exhibit distinct vibrational distributions in the high-frequency region, indicating that local bonding differences are also reflected in the lattice dynamics. Taken together, these results suggest that the bonding heterogeneity in Li_2YH_6 is manifested as a functional differentiation of superconductivity-relevant electronic states and high-frequency vibrational features, thereby providing a more specific physical basis for understanding the electron–phonon-coupling-related characteristics of this system and its relatively high Tc.

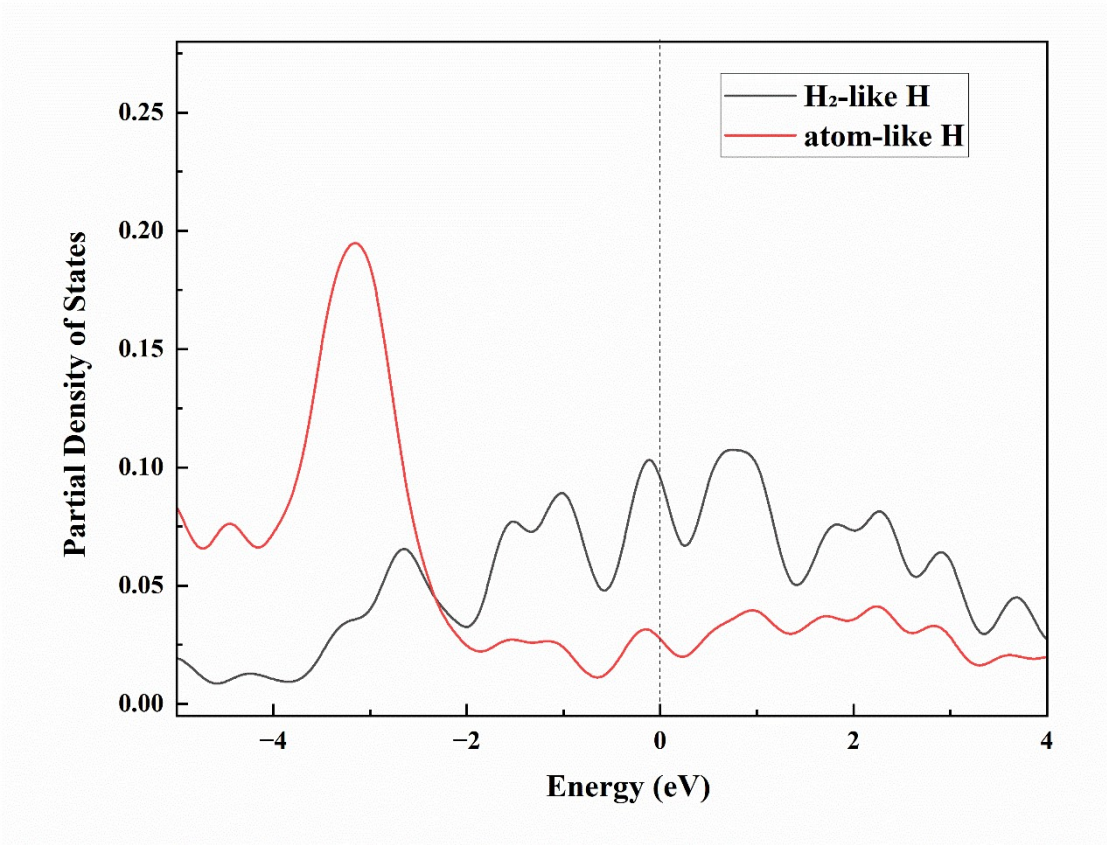

Figure S4. Partial density of states of representative H sites in Li_2YH_6 under 150 GPa. The PDOS of one representative H site in the H_2-like unit is compared with that of one representative atom-like H site. Since the two H atoms in the H_2-like unit are symmetry-equivalent and exhibit nearly identical PDOS features, only one representative H site is shown here. The Fermi level is set to 0 eV.

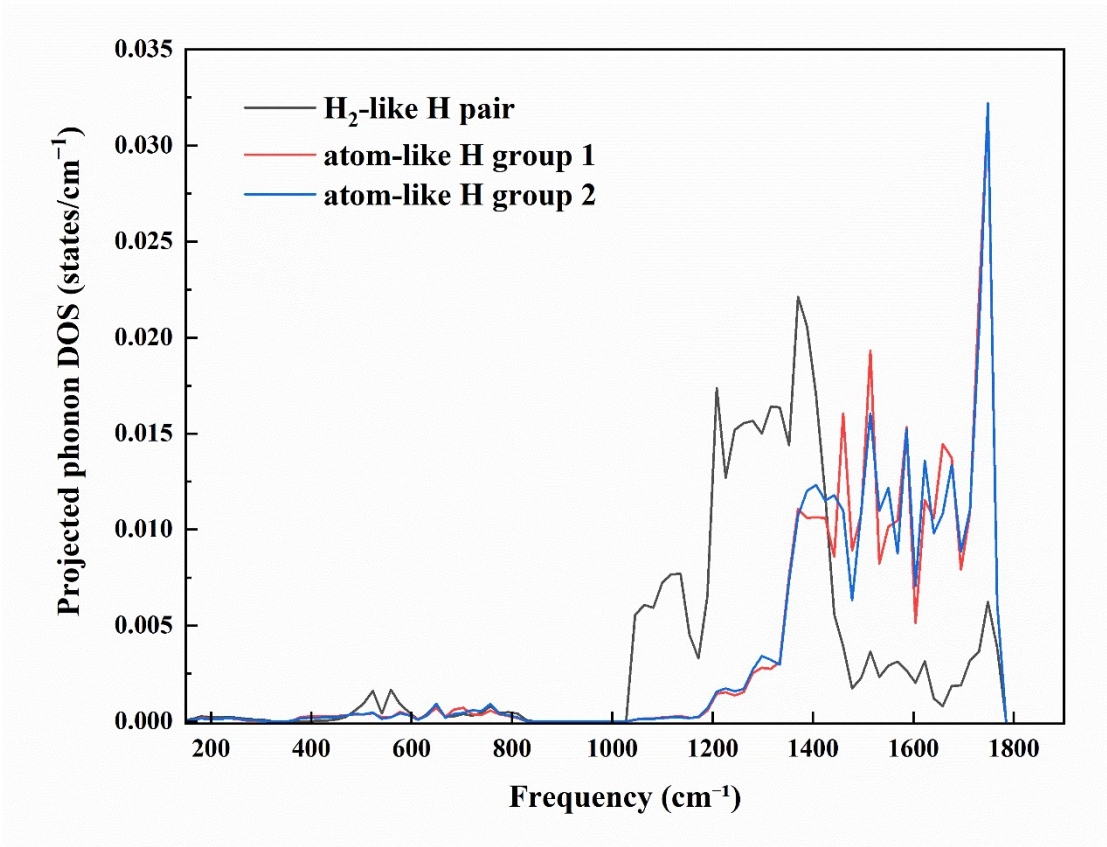

Figure S5. Projected phonon density of states of distinct local hydrogen environments in Li_2YH_6 at 150 GPa. The black curve corresponds to the H_2-like H environment, while the red and blue curves represent two inequivalent atom-like H environments. As shown, different local H environments exhibit clearly different spectral distributions in the high-frequency region. The horizontal axis denotes frequency, and the vertical axis represents the relative projected intensity.